PROCEEDINGS OF SPIE

Infrared Technology and Applications XLI

Bjørn F. Andresen
Gabor F. Fulop
Charles M. Hanson
Paul R. Norton
Editors

20–23 April 2015
Baltimore, Maryland, United States

Sponsored and Published by
SPIE

Volume 9451

Proceedings of SPIE 0277-786X, V. 9451

SPIE is an international society advancing an interdisciplinary approach to the science and application of light.

Infrared Technology and Applications XLI, edited by Bjørn F. Andresen,
Gabor F. Fulop, Charles M. Hanson, Paul R. Norton, Proc. of SPIE Vol. 9451,
945101 · © 2015 SPIE · CCC code: 0277-786X/15/$18 · doi: 10.1117/12.2184307

The papers included in this volume were part of the technical conference cited on the cover and title page. Papers were selected and subject to review by the editors and conference program committee. Some conference presentations may not be available for publication. The papers published in these proceedings reflect the work and thoughts of the authors and are published herein as submitted. The publisher is not responsible for the validity of the information or for any outcomes resulting from reliance thereon.

Please use the following format to cite material from this book:
Author(s), "Title of Paper," in *Infrared Technology and Applications XLI*, edited by Bjørn F. Andresen, Gabor F. Fulop, Charles M. Hanson, Paul R. Norton, Proceedings of SPIE Vol. 9451 (SPIE, Bellingham, WA, 2015) Article CID Number.

ISSN: 0277-786X
ISBN: 9781628415674

Published by
SPIE
P.O. Box 10, Bellingham, Washington 98227-0010 USA
Telephone +1 360 676 3290 (Pacific Time) · Fax +1 360 647 1445
SPIE.org

Copyright © 2015, Society of Photo-Optical Instrumentation Engineers.

Copying of material in this book for internal or personal use, or for the internal or personal use of specific clients, beyond the fair use provisions granted by the U.S. Copyright Law is authorized by SPIE subject to payment of copying fees. The Transactional Reporting Service base fee for this volume is $18.00 per article (or portion thereof), which should be paid directly to the Copyright Clearance Center (CCC), 222 Rosewood Drive, Danvers, MA 01923. Payment may also be made electronically through CCC Online at copyright.com. Other copying for republication, resale, advertising or promotion, or any form of systematic or multiple reproduction of any material in this book is prohibited except with permission in writing from the publisher. The CCC fee code is 0277-786X/15/$18.00.

Printed in the United States of America.

Publication of record for individual papers is online in the SPIE Digital Library.

SPIE Digital Library

SPIEDigitalLibrary.org

Paper Numbering: Proceedings of SPIE follow an e-First publication model, with papers published first online and then in print. Papers are published as they are submitted and meet publication criteria. A unique citation identifier (CID) number is assigned to each article at the time of the first publication. Utilization of CIDs allows articles to be fully citable as soon as they are published online, and connects the same identifier to all online, print, and electronic versions of the publication. SPIE uses a six-digit CID article numbering system in which:

- The first four digits correspond to the SPIE volume number.
- The last two digits indicate publication order within the volume using a Base 36 numbering system employing both numerals and letters. These two-number sets start with 00, 01, 02, 03, 04, 05, 06, 07, 08, 09, 0A, 0B … 0Z, followed by 10-1Z, 20-2Z, etc.

The CID Number appears on each page of the manuscript. The complete citation is used on the first page, and an abbreviated version on subsequent pages.

Contents

HOT: HIGH OPERATING TEMPERATURE FPAS

UNCOOLED FPAS AND APPLICATIONS I

UNCOOLED FPAS AND APPLICATIONS II

CRYOGENIC DETECTOR COOLERS

HGCDTE

A WORD FROM THE MASTERS

REDUCING THE PITCH

SMART PROCESSING 9451

ALTERNATIVE PHOTON DETECTORS AND APPLICATIONS

Authors

Numbers in the index correspond to the last two digits of the six-digit citation identifier (CID) article numbering system used in Proceedings of SPIE. The first four digits reflect the volume number. Base 36 numbering is employed for the last two digits and indicates the order of articles within the volume. Numbers start with 00, 01, 02, 03, 04, 05, 06, 07, 08, 09, 0A, 0B...0Z, followed by 10-1Z, 20-2Z, etc.

Conference Committee

Symposium Chair

Nils R. Sandell Jr., Strategic Technology Office, DARPA (United States)

Symposium Co-chair

David A. Logan, BAE Systems (United States)

Conference Chairs

Bjørn F. Andresen, RICOR-Cryogenic & Vacuum Systems (Israel)
Gabor F. Fulop, Maxtech International, Inc. (United States)
Charles M. Hanson, SenseIR Solutions, LLC (United States)
Paul R. Norton, U.S. Army Night Vision & Electronic Sensors Directorate (United States)

Conference Program Committee

Tayfun Akin, Mikro-Tasarim Ltd. (Turkey) and Middle East Technical University (Turkey)
Christopher C. Alexay, StingRay Optics, LLC (United States)
Stefan T. Baur, Raytheon Vision Systems (United States)
Philippe F. Bois, Thales Research & Technology (France)
Wolfgang A. Cabanski, AIM INFRAROT-MODULE GmbH (Germany)
John T. Caulfield, Cyan Systems (United States)
Eric M. Costard, SOFRADIR (France)
Ronald G. Driggers, St. Johns Optical Systems (United States)
Michael T. Eismann, Air Force Research Laboratory (United States)
Christy Fernandez-Cull, MIT Lincoln Laboratory (United States)
Mark E. Greiner, L-3 Communications Cincinnati Electronics (United States)
Sarath D. Gunapala, Jet Propulsion Laboratory (United States)
Masafumi Kimata, Ritsumeikan University (Japan)
Hee Chul Lee, KAIST (Korea, Republic of)
Paul D. LeVan, Air Force Research Laboratory (United States)
Chuan C. Li, DRS Technologies, Inc. (United States)
Kevin C. Liddiard, Electro-optic Sensor Design (Australia)
Wei Lu, Shanghai Institute of Technical Physics (China)
Tara J. Martin, UTC Aerospace Systems (United States)
Paul L. McCarley, Air Force Research Laboratory (United States)
R. Kennedy McEwen, SELEX ES (United Kingdom)
John L. Miller, FLIR Systems, Inc. (United States)

A. Fenner Milton, U.S. Army Night Vision & Electronic Sensors Directorate (United States)
Mario O. Münzberg, Airbus DS Optronics GmbH (Germany)
Peter W. Norton, BAE Systems (United States)
Robert A. Owen, L-3 Communications EOTech. (United States)
Joseph G. Pellegrino, U.S. Army Night Vision & Electronic Sensors Directorate (United States)
Manijeh Razeghi, Northwestern University (United States)
Donald A. Reago Jr., U.S. Army Night Vision & Electronic Sensors Directorate (United States)
Colin E. Reese, U.S. Army Night Vision & Electronic Sensors Directorate (United States)
Sergey V. Riabzev, RICOR-Cryogenic & Vacuum Systems (Israel)
Patrick Robert, ULIS (France)
Antoni Rogalski, Military University of Technology (Poland)
Ingo Rühlich, AIM INFRAROT-MODULE GmbH (Germany)
Jas S. Sanghera, U.S. Naval Research Laboratory (United States)
Itay Shtrichman, SCD Semiconductor Devices (Israel)
Torbjørn Skauli, Norwegian Defence Research Establishment (Norway)
Miguel P. Snyder, U.S. Army Night Vision & Electronic Sensors Directorate (United States)
Rengarajan Sudharsanan, Spectrolab, Inc., A Boeing Company (United States)
Stefan P. Svensson, U.S. Army Research Laboratory (United States)
Alan Symmons, LightPath Technologies, Inc. (United States)
J. Ralph Teague, Georgia Tech Research Institute (United States)
Simon Thibault, Université Laval (Canada)
Meimei Tidrow, U.S. Army Night Vision & Electronic Sensors Directorate (United States)
Alexander Veprik, SCD Semiconductor Devices (Israel)
Jay N. Vizgaitis, optX imaging systems (United States)
Michel Vuillermet, SOFRADIR (France)
James R. Waterman, U.S. Naval Research Laboratory (United States)
Lucy Zheng, Institute for Defense Analyses (United States)

Session Chairs

1 NIR / SWIR FPAs and Applications
Mario O. Münzberg, Airbus DS Optronics GmbH (Germany)
Eric M. Costard, SOFRADIR (France)

2 Infrared in the Service of the Navy I
James R. Waterman, U.S. Naval Research Laboratory (United States)

3 Infrared in the Service of the Navy II
James R. Waterman, U.S. Naval Research Laboratory (United States)

4 Infrared Imagers: Variations On a Theme
R. Kennedy McEwen, SELEX ES (United Kingdom)
Torbjørn Skauli, Norwegian Defence Research Establishment (Norway)

5 Infrared Imaging: Retaining Acquisition
Torbjørn Skauli, Norwegian Defence Research Establishment (Norway)
R. Kennedy McEwen, SELEX ES (United Kingdom)

6 Type II Superlattice FPAs I
Meimei Tidrow, U.S. Army Night Vision & Electronic Sensors Directorate (United States)
Manijeh Razeghi, Northwestern University (United States)
Lucy Zheng, Institute for Defense Analyses (United States)

7 Keynote Session
Paul R. Norton, U.S. Army Night Vision & Electronic Sensors Directorate (United States)

8 Type II Superlattice FPAs II
Meimei Tidrow, U.S. Army Night Vision & Electronic Sensors Directorate (United States)
John L. Miller, FLIR Systems, Inc. (United States)
Lucy Zheng, Institute for Defense Analyses (United States)

9 ROIC and NUC
Paul L. McCarley, Air Force Research Laboratory (United States)
John T. Caulfield, Cyan Systems (United States)

10 HOT: High Operating Temperature FPAs
Michael T. Eismann, Air Force Research Laboratory (United States)
Philip C. Klipstein, SCD SemiConductor Devices (Israel)

11 Uncooled FPAs and Applications I
Masafumi Kimata, Ritsumeikan University (Japan)
Stefan T. Baur, Raytheon Vision Systems (United States)

12 Uncooled FPAs and Applications II
Colin E. Reese, U.S. Army Night Vision & Electronic Sensors Directorate (United States)
Kevin C. Liddiard, Electro-optic Sensor Design (Australia)
Charles M. Hanson, SenseIR Solutions, LLC (United States)

13 Chalcogenide Glasses in IR Optical Design
Jasbinder S. Sanghera, U.S. Naval Research Laboratory (United States)
Christopher C. Alexay, StingRay Optics, LLC (United States)
Jay N. Vizgaitis, optX imaging systems (United States)

14 Alternative Approaches and Tools in IR Optical Design I
Jay N. Vizgaitis, optX imaging systems (United States)
Christopher C. Alexay, StingRay Optics, LLC (United States)
Jasbinder S. Sanghera, U.S. Naval Research Laboratory (United States)

15 Alternative Approaches and Tools in IR Optical Design II
Jay N. Vizgaitis, optX imaging systems (United States)
Christopher C. Alexay, StingRay Optics, LLC (United States)
Jasbinder S. Sanghera, U.S. Naval Research Laboratory (United States)

16 Cryogenic Detector Coolers
Richard M. Rawlings, DRS Technologies, Inc. (United States)
Sergey V. Riabzev, RICOR-Cryogenic & Vacuum Systems (Israel)
Ingo N. Ruehlich, AIM INFRAROT-MODULE GmbH (Germany)
Alexander Veprik, SCD SemiConductor Devices (Israel)

17 HgCdTe
Whitney Mason, U.S. Army Night Vision & Electronic Sensors Directorate (United States)
Michel Vuillermet, SOFRADIR (France)

18 A Word from the Masters
Paul R. Norton, U.S. Army Night Vision & Electronic Sensors Directorate (United States)

19 Reducing the Pitch
Ronald G. Driggers, St. Johns Optical Systems (United States)

20 Smart Processing
Paul L. McCarley, Air Force Research Laboratory (United States)
John T. Caulfield, Cyan Systems (United States)

21 Alternative Photon Detectors and Applications
Henk Martijn, IRnova AB (Sweden)

Introduction

The Forty-first conference on Infrared Technology and Applications was held April 20th-23th, 2015 at the Baltimore Convention Center in Baltimore, Maryland. The agenda was divided into 21 sessions:

1. NIR/SWIR FPAs and Applications
2. Infrared in the Service of the Navy I
3. Infrared in the Service of the Navy II
4. Infrared Imagers: Variations on a Theme
5. Infrared Imaging: Retaining Acquisition
6. Type II Superlattice FPAs I
7. Keynote Session
8. Type II Superlattice FPAs II
9. ROIC and NUC
10. HOT: High Operating Temperature FPAs
11. Uncooled FPAs and Applications I
12. Uncooled FPAs and Applications II

IR Optics I: Technologies and Design

13. Chalcogenide Glasses in IR Optical Design
14. Alternative Approaches and Tools in IR Optical Design I
15. Alternative Approaches and Tools in IR Optical Design II
16. Cryogenic Detector Coolers
17. HgCdTe
18. A Word from the Masters
19. Reducing the Pitch
20. Smart Processing
21. Alternative Photon Detectors and Applications

In addition, there were a number of poster papers presented for discussion on Tuesday evening—these have been added to the 21 sessions in the Proceedings. Highlights of six topical areas are summarized below:

- Photon Detectors
- Uncooled Detectors
- Optics
- Coolers
- Applications
- Keynote Address

Photon Detectors

NIR/SWIR FPAs and Applications

Near-infrared and shortwave infrared imaging—0.7 to 3 μm—continues to rise in popularity because of its ability to make use of sky glow to enhance performance during exceptionally dark periods of the night.

Development of SWIR FPAs is continuing in order to meet the needs of both military and commercial applications. Most of these developments make use of InGaAs, although new SWIR developments were also presented in thin film colloidal quantum dot (CQD) detectors and T2SL (Type II Superlattice) detectors.

The standard pitch for InGaAs FPAs is now 15 μm, with 12.5 μm and smaller also available. One system manufacturer described how the reduction in InGaAs pitch from 20 μm to 15 μm improved their multispectral vis/SWIR zoom camera. The lower pitch FPA had lower dark current and readout noise, which, together with an improved optics design, resulted in a noise equivalent irradiance reduction by a factor of three.

A manufacturer of InGaAs cameras showed the value of its smart image enhancement algorithms for a SWIR day and night vision camera. Figure 1 shows the improvements achieved.

Development on thin-film PbS Quantum Colloidal Dot (CQD) FPAs processed from solution has reached the point where they have been processed on a 640 × 512 ROIC with 15 μm pixels. A dark current of 2.7 nA/cm^2 was achieved at room temperature with a 10 mV bias. Devices with response to 2.2 μm have been demonstrated.

The potential for extended wavelength SWIR devices using Type 2 superlattices was explored by one company which fabricated three different structures based on InGaAs/GaAsSb/InP and one on an InPSb alloy. Good uniformity was obtained with a cutoff to 2.5 μm.

Fig. 1, SWIR image with Nonuniformity Correction (NUC) top, and with NUC, Automatic gain Control (AGC), and Histogram Equalization (HE) bottom.

Extended wavelength T2SL SWIR devices have been obtained by others and an FPA based on the technology was shown as a commercial product in the Exhibition.

Two papers describing enhanced CMOS imaging were presented. In the first, a low-noise 640 × 480/10 CMOS sensor was tested in the laboratory and shown to be comparable to a Gen III image intensifier under sub mLux starlight conditions.

In the second a "black silicon" layer prepared by ultra-fast laser processing is combined with low-noise CMOS image sensor design to provide enhanced sensitivity to 1.2 μm. Megapixel FPAs based on this design are capable of imaging at 60 fps in lighting conditions below 1 mLux with a latency of approximately 1 msec.

Type II Superlattice FPAs

There were a total of nine papers in the two sessions devoted to Type II Superlattice and Barrier detectors, and several more on this subject in the Poster session. This reflects the continued strong interest in the potential performance advantages that this technology has been predicted to have theoretically—long carrier lifetimes and a high optical absorption coefficient. Experimentally, lifetimes as long as those predicted have not yet been achieved, but improvements have been made recently for material structures that exclude gallium. Lifetimes continue to be shorter than for HgCdTe with comparable bandgaps. This year featured a larger focus on LWIR devices.

An overview of optimizing Type-II hetrojunction infrared detectors was presented first.

This was followed by an excellent presentation on LWIR Type II superlattice detectors using an XBp structure. Fig. 2 illustrates the XBp detector structure. A 640 × 512 array with 15 μm pixels has been developed having a 9.5 μm cutoff at 77 K. Fig. 3 illustrates the 13 mK NEΔT of at 78 K for a 65% well fill achieved by averaging 8 frames taken at 240 Hz for a net 30 Hz frame rate.

Theoretical and experimental investigation of SW/MWIR dual-band Type II detectors was presented. A barrier detector design showed advantages over of a *pin* structure.

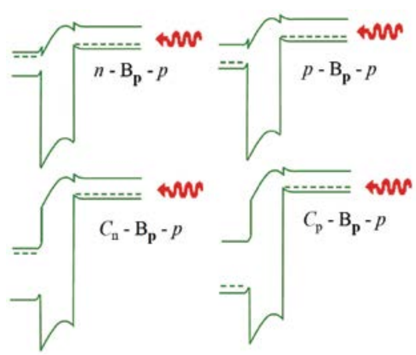

Fig. 2 Illustration of the variety of XBp detector band structure options.

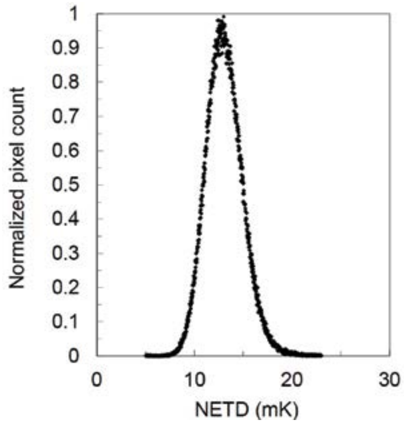

Fig. 3 NEΔT histogram of an XBp LWIR array with a 13 mK peak and no appreciable high noise tail.

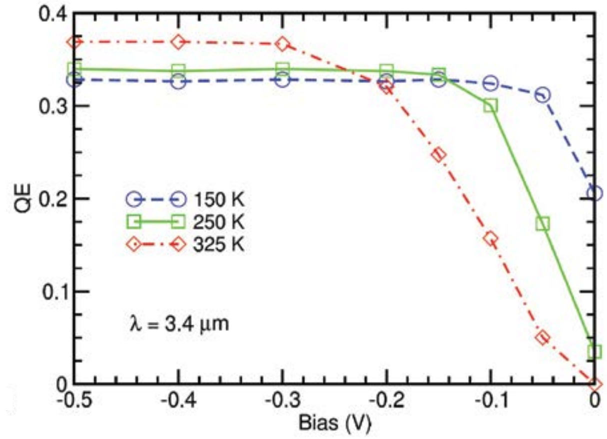

Fig. 5 QE measured at =3.4 μm as functions of bias at the temperatures indicated.

The interpretation that Type II InAs/GaSb homojunction detectors are limited by Schockly-Read-Hall centers was challenged in a paper that analyzed the current-voltage data from two LWIR Type II wafers over a wide temperature range. They attributed their analysis to show that shunt leakage was the limiting mechanism. Fig. 4 shows the shunt resistance for surface and area for one of the wafers.

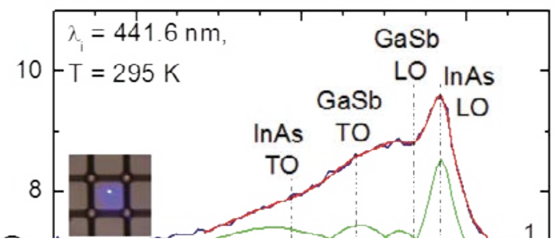

Fig. 6 Derived internal quantum efficiency of the MWIR and LWIR samples.

Carrier transport in unipolar barrier detectors based on Type II materials was discussed in the context of minority-carrier blocking and the potentially very low hole mobility in *nBn* structures. Fig. 5 illustrates the effect this can have on the bias voltage needed to saturate the quantum efficiency. Taking into account hole-mixing effects, the effective mass of holes may be lower than expected.

Photoluminescence as a function of laser power was used to study the lifetime of carriers in InAs/InAsSb Type II superlattice materials. Results were shown for both MWIR and LWIR samples. Data were relatively consistent with previous results. Quantum efficiency was also measured as shown in Fig. 6.

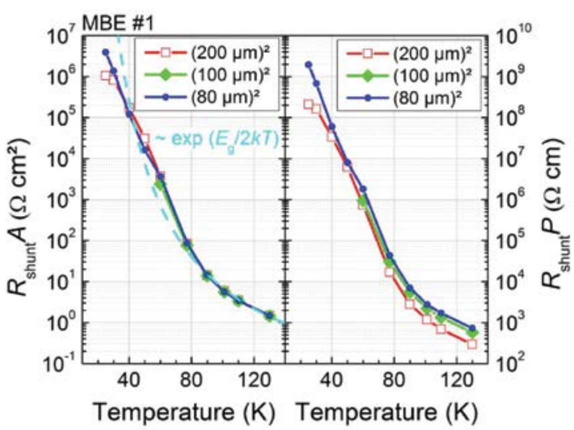

Fig. 4 $R_{shunt}A$ - and $R_{shunt}P$-products vs. temperature for three devices with different areas for MBE wafer #1.

Confocal Raman spectroscopy and atomic-force microscopy were used to study the sidewalls of InAs/GaSb Type II superlattice mesa detectors. One of the conclusions is that the sidewalls show considerable damage compared to the center of the 24 μm pixels. Fig. 7 shows the Raman spectra at different locations on a small portion of the array. Peak intensities are reduced on the sidewalls compared with the array center.

Development of 4-to-7-inch GaSb substrates was reported—Fig. 8 shows an example of the new, large boule size compared to 2-to-3-inch boules. In a subsequent paper, the successful growth of InAsSb/AlAsSb bulk *nBn* epitaxial detectors was demonstrated.

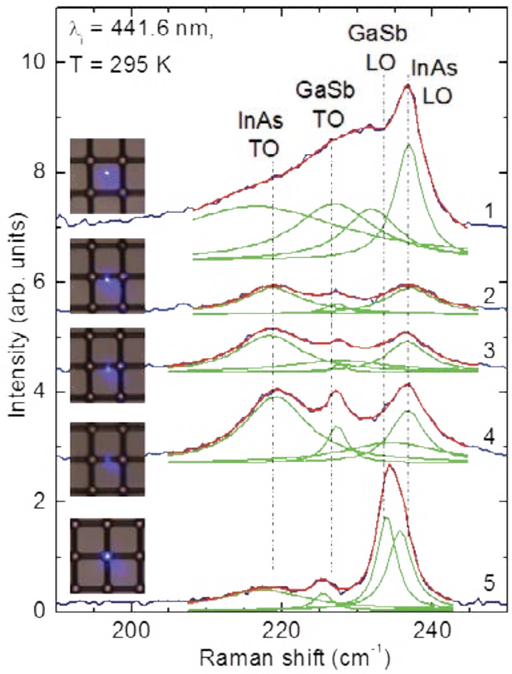

Fig. 7 Micro-Raman spectra of a T2SL-FPA structure measured at dierent points. Lorentzian tting was performed to distinguish dierent phonon features in the spectra (red lines { tting results; green lines { contributions from individual phonon modes). The inset images show the location of the laser spot corresponding to the measured spectra. Dashed lines are guides to the eye.

Fig. 8 Standard 2"/3" (left) and larger format 4"-7" (right) GaSb boules.

A final paper in this session reported on the IR transmission of large GaSb substrates as a function of doping. Transmission can be low in the VLWIR range when there is too much p-type doping due to absorption from transitions between the light- and heavy-hole bands. Te doping was used to partially compensate residual p-type dopants. Figure 9 illustrates how the IR transmission can vary with Te counter-doping.

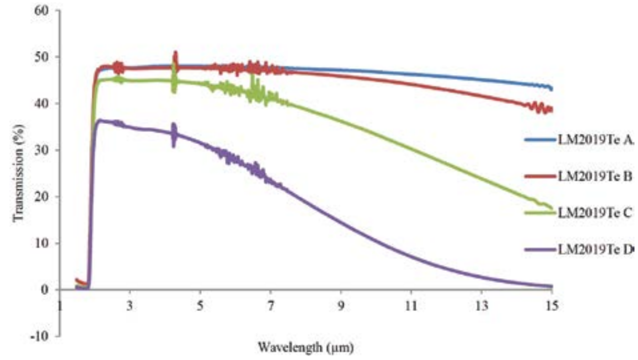

Fig. 9 Transmission measurement taken at the center point of slices A, B, C and D cut from boule LM2019Te.

ROICs and NUC

Three papers were presented describing readout designs. Three additional papers on this subject area were presented as posters. Readout designs included the following formats:

- A digital ROIC design was described for LWIR detectors suitable for either staring or scanning formats using a pulse frequency modulation that can accommodate > 2×10^9 charge storage per pixel—equivalent to 20 bits in a 30 μm unit cell.

- A SWIR ROIC featuring a CTIA input in a 1280×1024 format with 15 μm pitch was reported. On-chip provision for bias and timing is included. Noise is < 5 e- in the very high gain mode. Fig. 10 shows modular USB-based camera electronics based on this design.

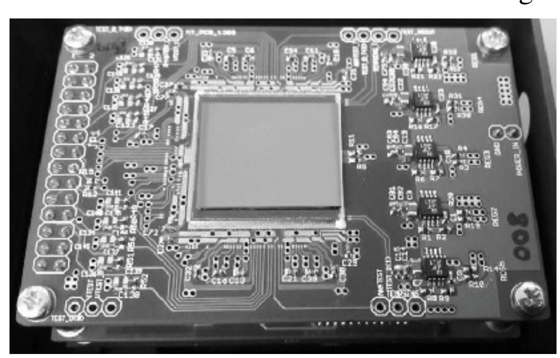

Fig. 10 Modular USB based camera electronics

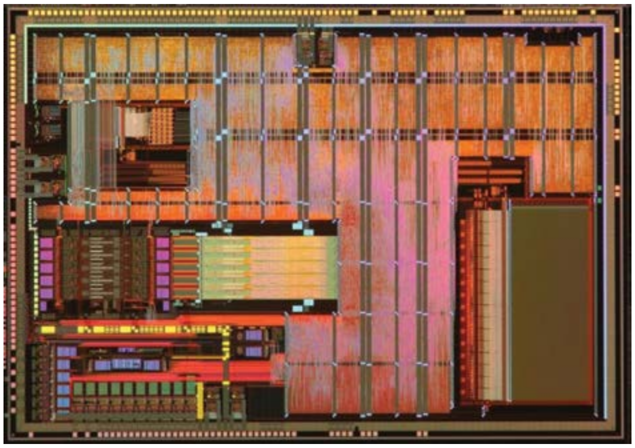

Fig. 11 NIRCA is produced in an AMS 0.35 µm CMOS process

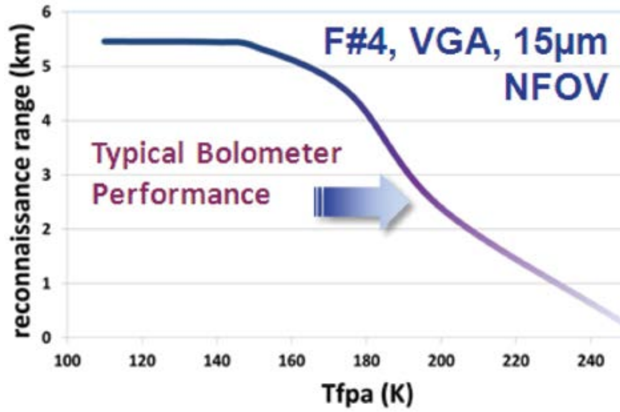

Fig. 12 Range performance of a HgCdTe FPA with narrow-field optics vs. operating temperature. The arrow shows the typical microbolometer performance of 2.5 km.

- Cryogenic measurements of the digital pixel design described in the first bullet above were made to evaluate the design.
- Low-voltage differential signalling was proposed for linking an FPA to a microprocessor input.
- An uncooled microbolometer readout was described in a 640 × 480 format with 17 μm pixels.
- An ASIC— Near Infrared Readout and Controller (NIRCA)—was unveiled to provide a generic interface between FPAs and a master system controller. Fig. 11 shows an image of the ASIC chip.

High Operating Temperature (HOT) FPAs

The goal of increasing the operating temperature of FPAs without sacrificing performance is motivated by the reduction in cooler power, improved cooler efficiency, longer cooler lifetime, smaller imager size, and lighter weight sensor systems that this makes possible. This goal is being pursued using HgCdTe, Type II superlattices, and *nBn* materials and has relevance especially in the MWIR and LWIR spectral bands.

An extensive and detailed paper on the trade-offs of Size, Weight, and Power (SWaP) considerations for cooled FPAs was presented with extensive analysis. Fig. 12 shows how the detection range varies with operating temperature for an MWIR HgCdTe array using narrow field-of-view f/4 optics as a function of operating temperature. The cooled FPA has greater range for temperatures below about 195 K.

High operating temperature HgCdTe detectors featuring enhanced functionality were described in another paper. Fig. 13 shows the weight advantages of HOT MWIR detectors compared to microbolometers. Fig. 14 illustrates imagery that can be bring out subtle details in the imagery using local-area contrast enhancement.

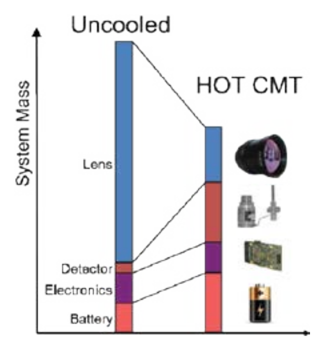

Fig. 13 Weight reduction of HOT HgCdTe compared to uncooled

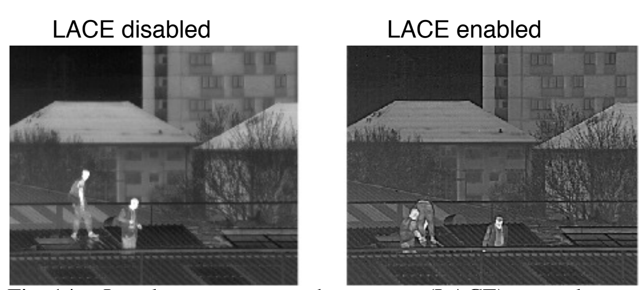

Fig. 14 Local-area contrast enhancement (LACE) example.

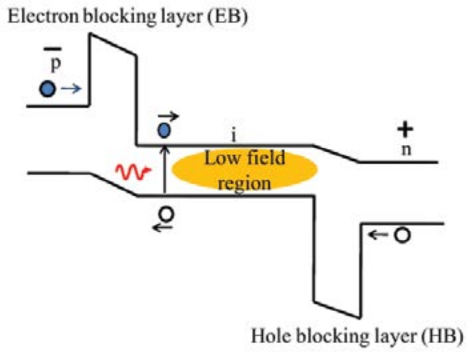

Fig. 15 Band diagram of the pBiBn device, which illustrates how the unipolar barriers block the flow of minority carriers. Note that if the barriers are designed correctly, the photocarriers are not impeded by the barriers.

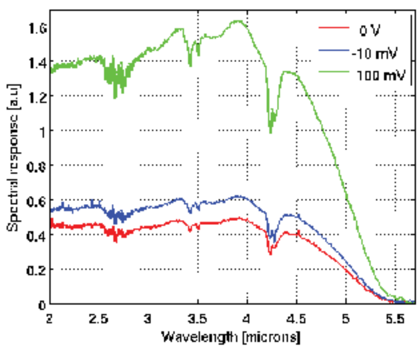

Fig. 16 Spectral response at 200 K. The 50% cutoff wavelength is around 5.04 μm.

Another HOT paper reported on MWIR unipolar barrier detectors based on Type II superlattice material in a *pBiBn* configuration illustrated in Fig. 15. Spectral response for this device at 200 K is shown in Fig. 16.

The effects of AlSb barriers on the properties of InAs/InAsSb superlattice material properties were explored in a paper on photoluminesce and Hall effect properties Samples with two (VL17), one (VL19), and no AlSb barriers (VL18) were studied. Mobility at 10 K was considerably reduced for the sample with barrier—see Fig. 17.

Interband cascade photodetectors were reviewed as HOT detector candidates for both MWIR and LWIR bands. Significant progress over the past year was reported. Fig. 18 illustrates the MWIR spectral D* for a wide range of temperatures and Fig. 19 shows the LWIR spectral D*.

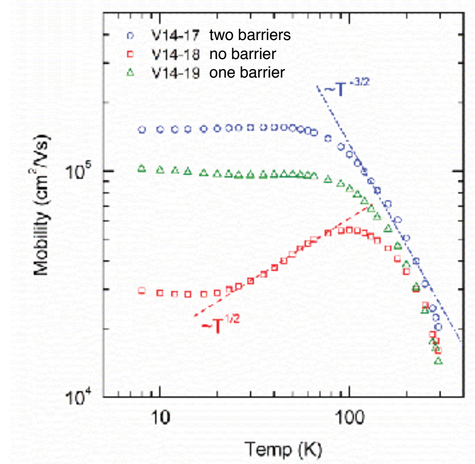

Fig. 17 Temperature-dependent mobility for samples with two, one, and no AlSb barriers.

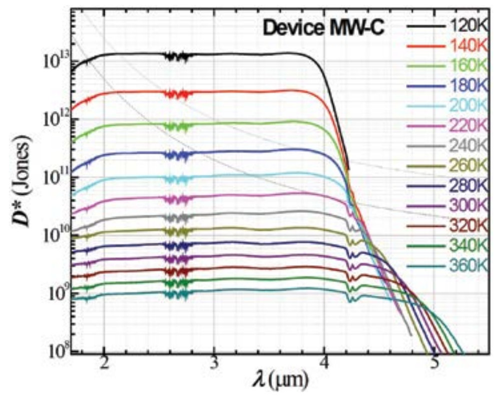

Fig. 18 Johnson-noise limited D* spectra of mid-IR IC detectors sample MW-C. The dashed lines represent the background-limited performance (BLIP) D* for a photovoltaic detector with an external QE of 70%, and the dotted lines are the BLIP D* for 5-stage devices with absorption QE of 70%, both under 300 K background with 2π field of view (FOV).

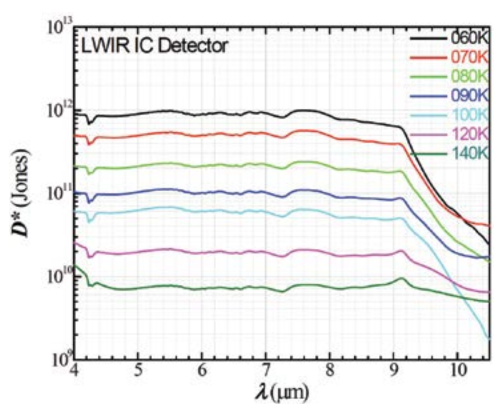

Fig. 19 Johnson-noise limited D* spectra of LWIR IC detectors at various temperatures.

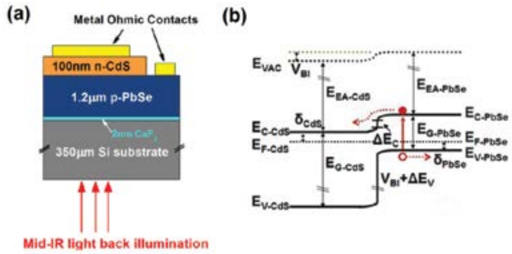

Fig. 20 (a) Schematic of the CdS/PbSe heterojunction photodetector; (b) Energy band diagram of n-CdS/p-PbSe heterojunction photodetector.

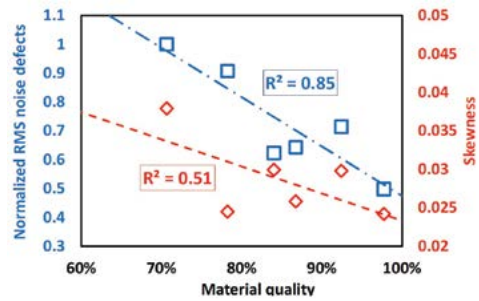

Fig. 22 Skewness and defective pixels calculated thanks to the 1.5.median criterion as a function of epilayer material quality. Each point is the median of several devices having same material quality.

CdS/PbSe heterojunction detectors were the subject of the final paper in the HOT session. This topic was explored using a one-dimensional model to determine the key variable that can improve the device structure illustrated in Fig. 20. These materials have very low Auger recombination rates compared to other IR detector materials and thus have great potential for HOT applications.

HgCdTe

The HgCdTe alloy detector—characterized by a high absorption coefficient and a long lifetime—continues to dominate the choice for a broad range of infrared applications. Aside from applications that are ideal for either InSb in the MWIR spectral band, or InGaAs in the 1.7 μm SWIR band, or those that can utilize uncooled FPAs, HgCdTe continues to be the most popular choice. Papers in this section update how HgCdTe is continuing to develop and evolve. Papers on this topic were presented one session on HgCdTe detectors as well as in the HOT session, the Applications sessions, and in the Poster session.

RMS noise modeling of MWIR and LWIR HgCdTe FPAs has been studied in order to be able to model the main distribution of background limited diodes and those with elevated noise due to 1/f defects. Noise histograms were reviewed using linear, log, and cumulative density plots as illustrated in Fig. 21. This was correlated with material quality as shown in Fig. 22. and used to improve the overall quality of FPAs.

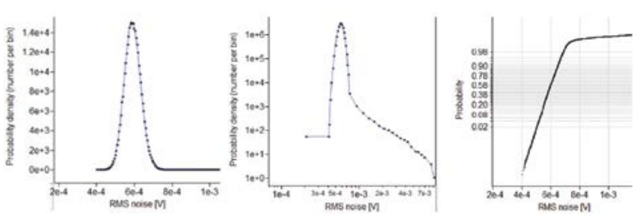

Fig. 21 Detector noise probability density in linear-linear scale, in log-log scale and the cumulative density in a normal Y scale.

MBE-grown HgCdTe on GaAs substrates was the subject of another paper. Results from single-color MWIR and LWIR were reviewed, and also MWIR/MWIR two color devices. Fig. 23 shows an SEM image of dual color pixels that has an *npn* structure.

Improvements in HgCdTe FPA performance were described, including pixel pitch reduction from 20 to 10 μm. LPE material was used. Fig. 24 illustrates how the NEΔT improves with integration time/charge storage capacity.

LPE HgCdTe was evaluated for space applications in the LWIR/VLWIR range (10 - 17 μm) using a p-on-n device structure. Results were improved over n-on-p structures that relied on vacancy doping. Quantum efficiency decreased below ~ 50 - 60 K.

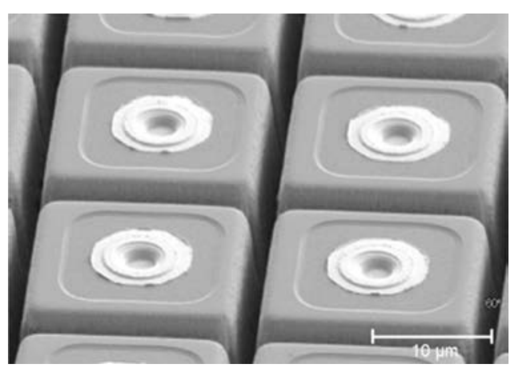

Fig. 23 Image of mesa-etched two-color pixels in a 640 × 512 pixel array with 20 μm pitch.

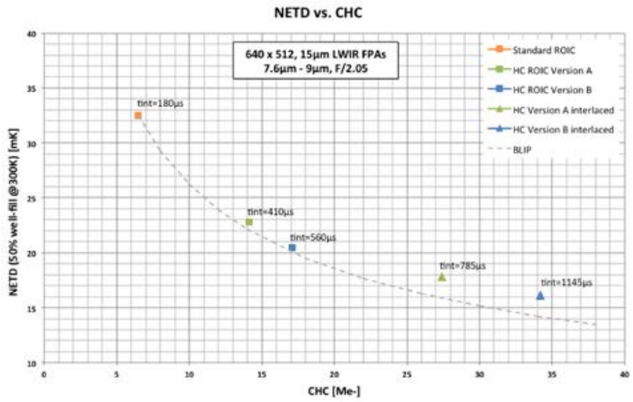

Fig. 24 NEΔT vs. charge handling capacity for a LWIR 15 μm pitch HgCdTe FPA. Integration time is also noted on the data points.

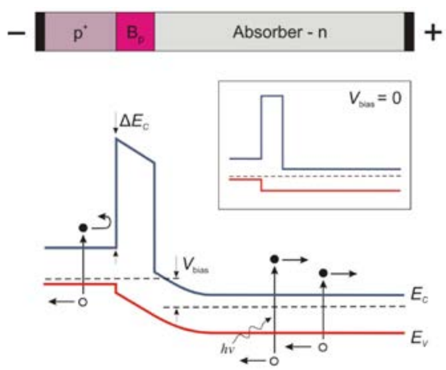

Fig. 28 Schematic band diagram of a HgCdTe barrier detector with zero valence band offset.

A paper described HgCdTe HOT detectors for MWIR operation with an nB_nn structure as shown in Fig. 25. Data from the first samples was presented and compared with Rule 07.

The thermal stability of Al_2O_3 films on HgCdTe were reported in the final paper of this session.

Word from the Masters

We enjoyed two presentations by distinguished members of the IR detector community who have recently retired. The first was Michael Kinch from DRS—formerly Texas Instruments. Mike described his career in detector technology (paper included in the proceedings).

Fig. 26 Depiction of a French castle under siege. No information was provided on the treasure it may hold.

The second talk was by Gérard Destefanis who talked about his career in HgCdTe in France—inside a HgCdTe castle with a growing number of threats—see Fig. 26. Gérard talked about the development of HgCdTe in France, the current state-of-the-art, and the challenges from competing technologies.

Reducing the pitch

Smaller pitch HgCdTe FPAs was the topic of one session. The challenges associated with obtaining small pitch— ~5 μm —were outlined, including:

- pixel delineation
- pixel hybridization
- unit cell well-capacity
- dark current

MOVPE-grown HgCdTe array development with reduced pitch was discussed. Fig. 27 shows the evolution of MOVPE HgCdTe pixel shrinkage. New arrays with 8 μm pitch for MWIR applications were presented along with an NEΔT histogram.

10 μm pitch FPAs were also reported in a second paper in this session. Fig. 28 illustrates the improvement in range for the 10 μm pixel referenced to an earlier design with 15 μm pitch.

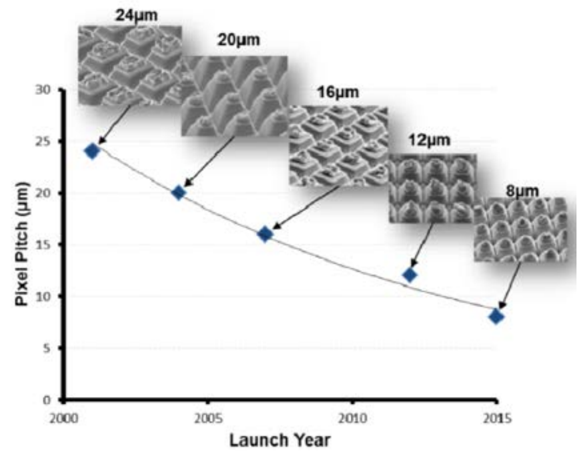

Fig. 27 Evolution of pixel reduction for MOVPE-grown HgCdTe.

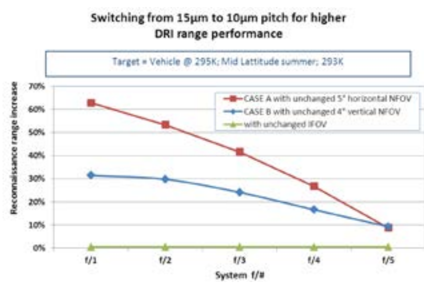

Fig. 28 Reconnaissance range for 10 μm pixels as a function of system f/# compared to 15 μm reference.

Very small–5 μm—pixels were unveiled in a paper featuring a 2040 × 1156 format InAsSb HOT MWIR array. Fig. 29 shows an image from a laboratory camera with this FPA. Details of the advantages of oversampling were described in some examples.

Fig. 29 Image from a HOT MWIR InAsSb array with 5 μm pixels in a 2040 × 1156 format.

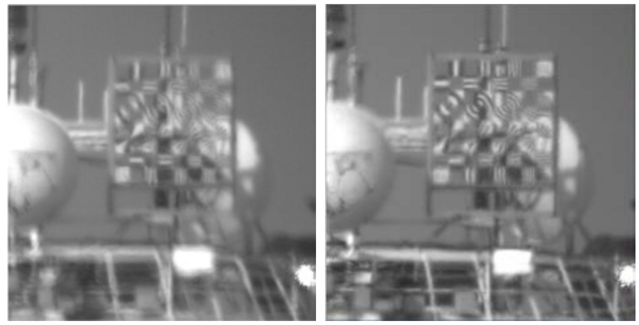

Fig. 30 left - unprocessed video; right - GPU version of LRF using Gaussian blur filter radius 4 and standard deviation 1.5.

Smart processing

One paper was presented in the smart processing session. The subject was on improving image clarity when looking through turbulence. Certain regions of a frame may be relatively clear, with the relatively-clear region varying from frame to frame. The paper described assembling an enhanced image from a collection of frames with- relatively clear or "lucky" regions (LRF). Hardware—a graphics processing unit (GPU)—was used to accelerate this collection. Fig. 30 illustrates the improvement in image clarity.

Alternative photon detectors and applications

There were two QWIP papers in this session. The first was an update on resonator QWIP development. Electric field effects were modeled as illustrated in Fig. 31, and their impact on quantum efficiency was used to calculate FPA performance.

The second QWIP paper reported on theoretical considerations of FPA uniformity. The impact of nonlinearity in the electronics is illustrated in Fig. 32.

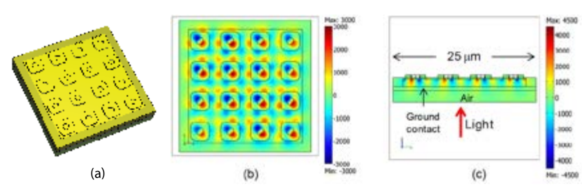

Fig. 31 (a) The 3-d perspective, (b) top view and (c) side view of the present R-QWIP design. The figure also shows the Ez distribution at λ = 9.5 µm with α = 0 (b) on the center plane of the active layer and (c) on the center plane of the second ring column. The incident E0 is 533.2 units. The pixel pitch is 25 µm, and the pixel linear size is 22 µm.

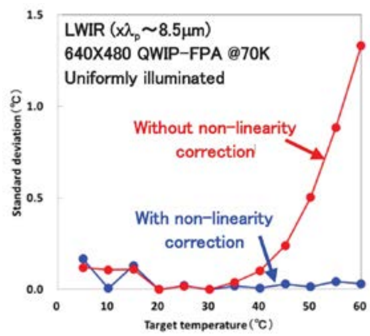

Fig. 32 Comparison of QWIP NUC results with and without non-linearity correction

Uncooled Detectors

The availability of uncooled IR microbolometer technology continues to expand. The number of manufacturers seems to be ever increasing, and the distribution of those producers is spreading across the globe. Size, weight, power and cost, raisons d'être for uncooled IR, continue to shrink.

The first two papers of the uncooled sessions presented to the Western world for the first time the progress of uncooled IR detector and system technology development in China, from the industrial point of view. Vanadium Oxide (VOx) and amorphous silicon (a-Si) are both in production. VOx arrays are available in arrays ranging from 160 × 120 to 640 ×5 12 with pixel sizes ranging from 45 μm down to 20 μm. A-Si arrays range from 160×120 to 640 × 480 with pixels sizes from 35 μm to 17 μm. Typical specified NEΔTs are in the 50 – 60 mK range for the smaller pixel sizes.

Two U.S. companies have made remarkable strides in reduction of size and cost of uncooled IR cores and systems. VOx arrays are being packaged at the wafer level to reduce size and cost, and pixel pitch is down to 12 μm. Custom ICs further reduce size, weight and power. In one case, a IR sensors are available that plug directly into the micro-USB port of Android and iOS phones, as shown in Fig. 33. In another instance, the entire sensor, including optics, is a stacked-chip assembly directly integrable into a smart phone, as shown in Fig. 34.

Fig. 33 Seek WFOV and NFOV (XR) thermal cameras are available for both iOS and Android

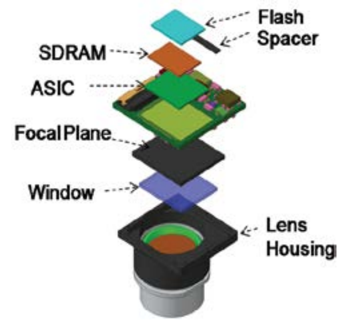

Fig. 34 SMART Chip camera schematic

Japan placed a compact uncooled infrared camera in orbit as a technology demonstration payload and evaluated its performance using targets of opportunity on the earth's surface. Methods were established to evaluate both MTF and radiometric quality. The camera was shutterless.

Papers from Israel, Belgium and Germany addressed shutterless operation of uncooled IR cameras. Innovations discussed include improved nonuniformity analysis and calibration, scene-based NUC, noise-reduction algorithms and improved dynamic range compression. Performance remains somewhat degraded relative to sensors having a well-designed shutter mechanism, but the gap is closing, and performance is adequate for many applications.

Meanwhile, a U.S. company has developed shutters with embedded microprocessors. Shutters are used to provide a uniform scene of relatively constant temperature for real-time uniformity correction. It is desirable to minimize the transmission time in order to maximize the time available for calibration while minimizing interruption of imaging. Embedding a microprocessor in the shutter permits efficient control blade motion for rapid transitions with minimal power. Three papers addressed enhancement to IR absorption in bolometric detectors. Two of these were from Japan and one from the U.S., and all were cooperative efforts between industry and academia. The U.S. paper investigated enhanced absorption by use of a pattern gold black absorber, stabilized with a protective evaporated oxide. The two Japanese papers described plasmonic absorbers, one of which provided photolithographic tuning of spectral response, and the other of which, a poster paper, provided selective polarization, also photolithographically.

A poster paper from Turkey described metal-insulator-metal (MIM) diodes for rectification of antenna-coupled IR detectors. In these devices an antenna responds to IR radiation by producing currents in the THz range. MIM diodes provide more efficient rectification than junction diodes, which increases the effective quantum efficiency of the detector. The design of the MIM device included an aluminum layer beneath an Al_2O_3 insulator layer. The top metal was chromium overlaid with gold. The design achieved quantum efficiencies as high as 29%.

Uncooled IR technology is very mature – even commoditized – in many ways; yet, innovation continues. Pixel sizes are approaching the practical limit, but continued performance enhancements could extend that limit. It seems certain that new applications and more demanding requirements will continue to drive new developments.

Optics

The subjects of the three IR Optics sessions, 13 – 15, are essentially divided into two. The first part reports on chalcogenide optical materials and their use in optical system design while the second part discusses alternative approaches and tools in IR optical design.

Multispectral and hyperspectral systems are required to increase target acquisition performance as well as to answer SWaP-C requirements for military and paramilitary systems. While today's FPAs can potentially enable compact, lightweight multiband spectral systems, there are few optical materials covering the SWIR – LWIR transmission range. The result of this is that several optical components are needed to correct for chromatic aberrations over a broad wavelength spectrum – adding size and excessive weight to the systems.

Several laboratories have lately presented results of their efforts to fill up the infrared glass map – closing

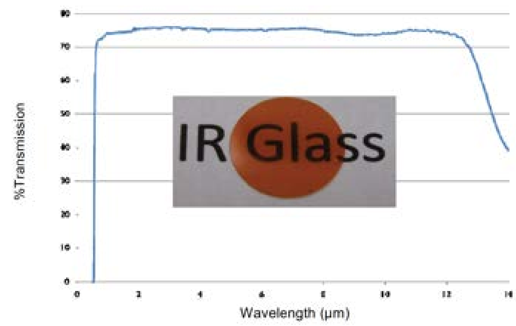

Fig. 35 Broadband IR transmission of a typical IR glass.

the many gaps in the refractive index values – in order to enable compact multiband optical systems. Foremost among these is the U.S. Naval Research Laboratory. A full session was devoted to recently developed chalcogenide materials and their use in optical designs. Fig. 35 shows a typical transmission plot of an NRL chalcogenide glass. The glasses are amenable to single point diamond turning for complex surfaces and molding for low cost volume production. One presentation pointed out that an added advantage in using these materials is that the glasses may be bonded. This results in a reduction of the number of air/glass interfaces. Examples were given of layered and bonded optics.

Another presentation from the same laboratory described use of chalcogenide glasses for making IR GRIN (Gradient Refractive Index) optical elements. These elements have tailored index variations that manipulate and control the radiation path within the bulk of the material. As the elements are designed with simultaneous optical power and chromatic correction a reduction in the number of elements in a wideband optical system is possible. Fig. 36 shows the IR GRIN process with diffusion and, alternatively, with bonded layers.

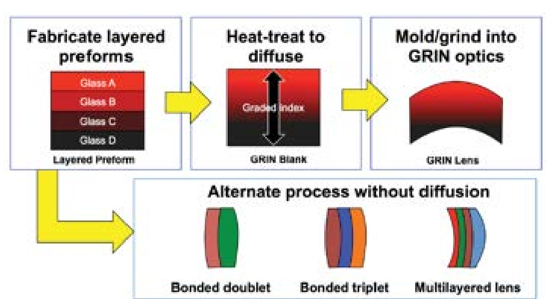

Fig. 35 IR GRIN process overview. Top: with diffusion. Bottom: with bonding.

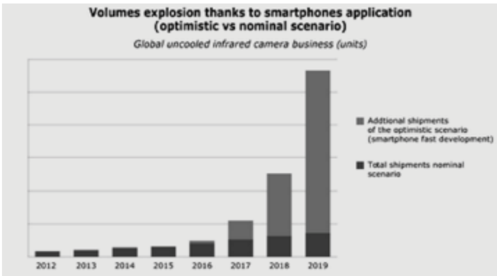

Fig. 37 Consumer IR imaging market prediction.

One company discussed their efforts to reduce the cost of chalcogenide glass optics for high-volume thermal imaging lenses. Following their thorough study where they compared the properties of germanium-free $As_{40}Se_{60}$ with the more expensive $Ge_{28}Sb_{12}Se_{60}$, they concluded that the former offers promising potential for improved thermal performance and lower cost for high volume consumer applications.

Another company explored the production process for affordable chalcogenide lenses from design to manufacture. Fig. 37 illustrates the expected growth of consumer demand.

One company provided an exciting example of how GRIN materials can provide an answer to a common problem like narcissus in imaging systems. Narcissus is caused by reflection of the cold stop off a lens surface back to the image plane of a cooled infrared system. The system's narcissus can be greatly reduced by changing the shape of one or more of the lenses. These changes will, however, in many cases also change the first order parameters and MTF of the original optical system. The presenter demonstrated that by employing GRIN materials in one or more of the component lenses, the original first order parameters and MTF may be retained for the near narcissus-free optical system.

Two presentations addressed testing of chalcogenide and GRIN optical elements. Both destructive and non-destructive means of measuring the GRIN index profile were investigated. Destructive testing involved slicing the optic. Non-destructive methods aim to correlate physical properties with the index of refraction. Both Raman mapping and CT scanning were used. Another non-destructive method for calculation of the refractive index is based on prism refractometery.

Among the alternative approaches in part 2, diffractive optics has not been accorded a separate presentation in our earlier sessions. The reason for this is that the use of diffractive optical elements, DOEs, in imaging has been limited. It is now realized that diffractive optics provides system developers and optical designers with additional flexibility in systems' architectures, resulting in solutions with reduced overall size and weight, as well as enhanced performance characteristics. One company discussed single and dual band optical systems based on non-chalcogenide materials. In one example the use of DOEs reduced the axial length and the weight of the system by factors of 2 and 3, respectively—see Fig. 38.

One company offered advice to fearful optical designers wishing to design a dual broadband VIS-SWIR diffraction-limited zoom lens system. It was pointed out that a set of diffraction-limited modules does not ensure diffraction-limited performance of the zoom lens. The inherent aberrations from one module can interact with aberrations from another module and cause induced aberrations which vary as the positions of the modules change through zoom. (Your editor was not altogether freed of varo-achro-phobia. See note at end of these optics reviews).

A company, well known for its mirror design and manufacturing, discussed its efforts to reduce SWAP-C of reflective optical systems for aerospace and defense applications. Minimizing the number of elements in the optical system was recognized as the obvious starting point for size and weight reduction. Diamond ma-

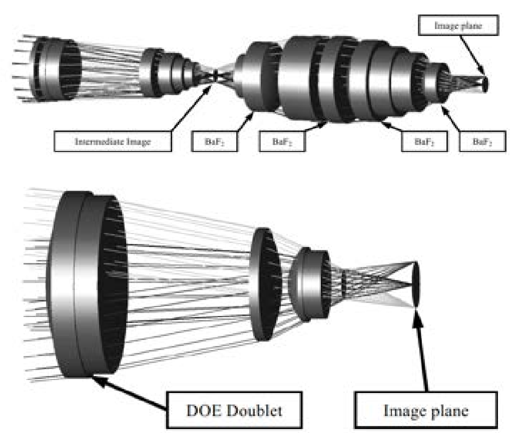

Fig. 38 Dual band IR objective without (top) and with (bottom) diffractive optical elements.

chining was considered for incorporation of aspheric/freeform surfaces which would enable elimination of elements. Other important factors considered were structural optimization, substrate stiffness and density, as well as surface finish quality. The same company reported on a new ultra-low surface finishing process for their aluminum mirrors. This finishing was applied to a 13 inch diameter parabolic mirror.

As modern IR/EO systems become more complex and the lines between optical and mechanical software become more blurred, there is a need for both optical and mechanical software to develop software-agnostic links to enable users to fully benefit from the advantages of each software suite. One company presented their software-agnostic process that does not depend on optical or mechanical software or plugins.

Note on next year's Infrared Optics sessions:

These sessions will be expanded and absorbed in a new DSS conference – Advanced Optics for Defense Applications – UV through LWIR.

Coolers

Infrared systems mounted on a soldier's weapon or in a small UAV need to be small, light and require low power. Cooled detectors operating at high temperatures up to 150 K and above (HOT) require less power hungry coolers than detectors cooled to 77 K temperature. See example in Fig. 39. A cooler drawing less power is usually smaller and lighter as well.

Two companies addressed HOT mechanical cryocoolers of both linear and rotary types. One company conducted trade-off analysis, mainly at system level, between start-up time, power consumption and reliability needs. Their linear cooler used a moving-magnet dual opposed-piston compressor which, combined with a free displacer cold finger, was effective in the application of active vibration reduction measures. Fig. 40 shows an example of regulated power vs. displacer length at 150 K for a HOT rotary cooler.

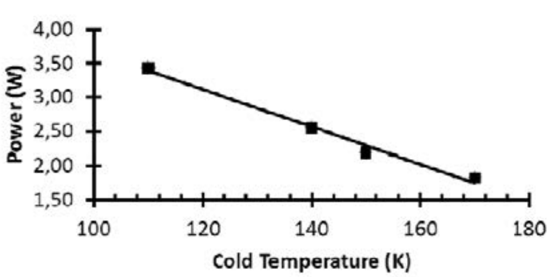

Fig. 39 Regulated power vs. cold temperature for a rotary cryocooler.

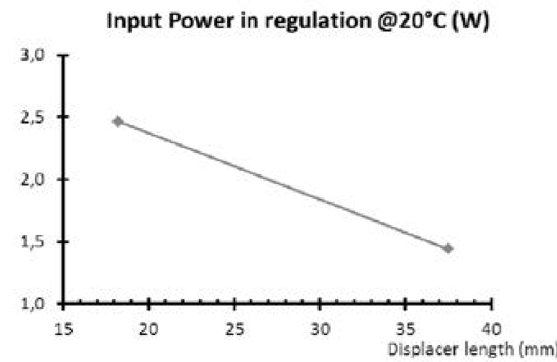

Fig. 40 Regulated power vs. displacer length for a rotary cryocooler at 150 K.

The other company defined as their goal for the rotary cooler a regulated power consumption down to 2 W DC for a cooling temperature of 150 K. The results shown in Fig. 41 were obtained by using a new high-efficiency motor and a thinned and shortened cold finger that reduce the self-heat loads. Stirling cycle simulation software was used in the performance optimization process.

A complete refrigeration system fundamentally consists of a thermodynamic device, like a mechanical, optical or thermo-electrical cooler, and the electronics to drive the device. Even the simplest of applications require a power source and a precision temperature control servo. Both of the two HOT cryocooler presentations discussed their miniaturized drive electronics. One pointed out the advantage of having dual

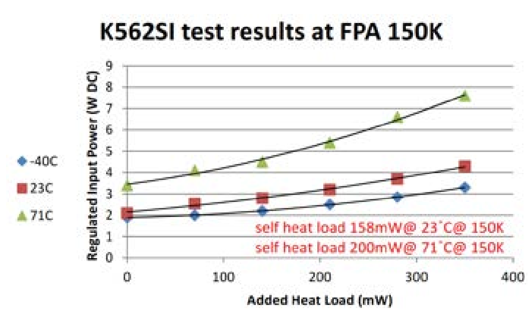

Fig. 41 Test results for an integral rotary HOT cryocooler.

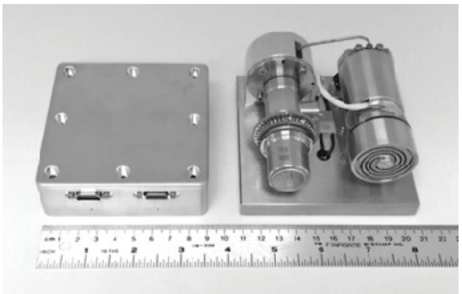

Fig. 42 Microsat cryocooler with its mLCCE electronics.

programmable set points. For high-flux scenarios an initial setting of the cooling temperature to 200 K will permit a faster cool-down.

Two companies focused on cryocoolers for specific applications. One discussed the development of a Microsat Cryocooler System with cooling capability of at least 0.5 W at a temperature of 140 K or below. Most of the report discussed the design of the radiation hardened miniature low-cost cryocooler electronics. This is recognized as the key technology requiring maturation to enable the objective missions. Fig. 42 shows a linear mechanical cooler and its electronics which together fit within the specified boundary of 10 cm x 20 cm x 6 cm.

One company reported on their development of cryocoolers required for operation under very harsh conditions. The specific application is for cooling the IR focal plane of a missile warning system mounted in a fighter aircraft, helicopter or a commercial airliner. One example of harsh environmental requirements was operation at temperatures between -46 C and +102 C and at random endurance vibration rates of 21.2 g rms. Test results showed that several of the company's cryocoolers have passed the qualification programs at system levels.

An elevated heat load of an Integrated Dewar-Detector Assembly (IDDA) may indicate a loss of vacuum due to natural outgassing, release of trapped contaminations or insufficient mechanical integrity. The evaluation of incoming heat flow has therefore become an important part of standard test procedures. The traditional method of heat flow measurement involves boil-off calorimetry. This is convenient for cryocoolers operating at 77 K, but for HOT coolers this method

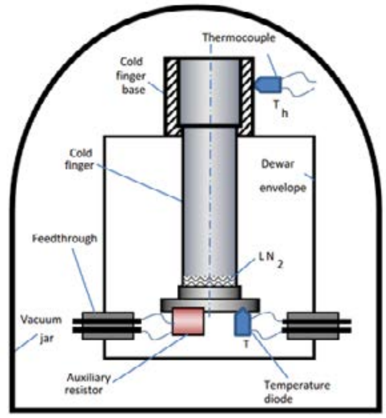

Fig. 43 Warm-up rate calorimetry set-up.

is not recommended due to inaccuracies, logistical difficulties and health and safety hazards. The proposed method of warm-up multi-slope calorimetry compares heating rates during warm up of an initially precooled cold finger in the IDDA, under different trial heat loads. Fig. 43 shows the experimental set-up.

Note on next year's Cryogenic Detector Coolers sessions:

> These sessions will be expanded and absorbed in a new DSS conference – Tri-Technology Device Refrigeration (TTDR). This conference will in addition to mechanical cryocoolers also include optical and thermo-electrical cryocoolers.

Applications

Presentations focusing on applications of the various infrared technologies in systems and subsystems were presented in Oral Sessions 2 - 5 and in the Poster Session. As applications are the main drivers for technology R&D, references to system applications can be found throughout the Proceedings.

The two Navy sessions, with updates from the first Navy session held in 2010, discussed potential impact of emerging imaging-related technologies on shipboard situational awareness and targeting systems. The challenges associated with the maritime environment and constraints associated with shipboard operation were considered.

Fig. 44 The opto-mechanically stabilized SPEED-LR payload.

Naval surveillance and reconnaissance systems, like IRST, require high spatial resolution in order to acquire small targets at long ranges. Development of focal plane arrays with high pixel count and small pixel pitch, together with near-diffraction-limited multiband optical subsystems, enable excellent resolution for systems mounted on stable, non-vibrating platforms.

Lack of good stabilization of platforms can easily reduce this resolution. A company with long experience in stabilization of their own and other reconnaissance systems discussed the relative merits of two means of stabilization – opto-mechanical and electronic – for imaging and non-imaging payloads against various scenes. Fig. 44 shows the company's long range, high resolution, observation payload with sub-pixel mechanical LOS stabilization.

One government institution discussed (presentation only) their maritime situational awareness and obstacle detection sensor system operating in the SWIR spectral band. A novel design achieves 360 degrees horizontal coverage with a single system having static FPA and objective optics. While employing an inverted multi-faceted pyramidal prism several azimuthal sectors are investigated with no image smearing or dead-time between observation of individual sectors. The design enables dual spectral sequential target search.

One company reported on their naval IRST which is based on the distributed aperture systems (DAS) concept for 360 degrees azimuth coverage. The purpose of the system is to detect and track maritime pirates at relatively short ranges.

Fig. 46 Absorption spectra of 0.2 mm thick sulfur copolymers samples.

The imager for a soldier's weapon sight is required to acquire targets at day and night. Low SWaP-C is another strong requirement. The first requirement calls for two sensors – one sight optimized for day and one for night. Having the two sensors mounted side-by-side will result in a heavy and clumsy sight which will slow the soldier carrying out his task. Changing and re-boresighting the sensor when light conditions change is another solution rejected by soldiers.

A company – a co-leader in the field - discussed the need for Clip-On In-Line Weapon Sights which answer all the above-mentioned requirements. After reviewing the evolution—see Fig. 45—of this type of weapon sights, the company outlined their plans for future development of their clip-on sights – developments that will further decrease SWaP-C and assure longer target acquisition ranges.

Military vehicles with small payload capacity, such as Unmanned Aerial Vehicles (UAV), require sensor systems with small volume, low mass and low power consumption (SWaP) while exhibiting target acquisition at long ranges. One company demonstrated a unique answer to these challenging requirements. Their approach consists of integrating the IR optical system inside the cold shield of the Detector Dewar Cooler Assembly (DDCA). A demonstrator system, having a low NETD due to cooling of the optics, was presented—see Fig. 46. The total optical track length of the miniaturized camera is only 3.8 mm. Applica-

Fig. 45 Evolution of clip-on sniper weapon sight technology over a 50 years period.

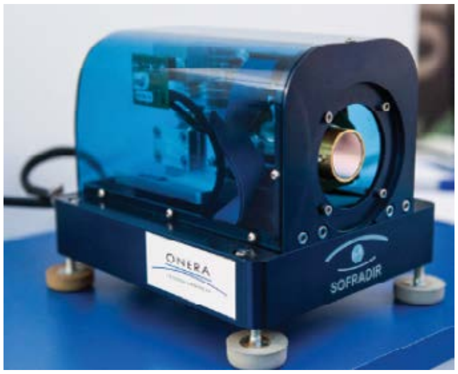

Fig. 46 Illustration of the IR ultrathin camera mounted in a demonstrator.

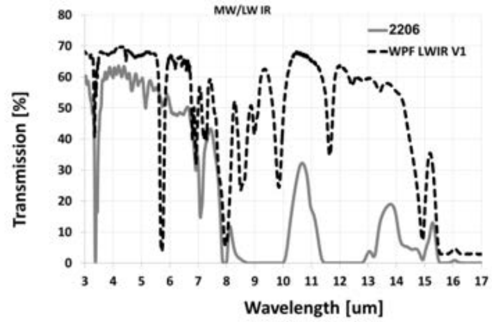

Fig. 48 Dual band WPF transmission without AR coating. 2206: earlier attempt. V1: recent result.

tions like wide FOV reconnaissance, multi- or hyperspectral imaging and others are envisaged.

A government laboratory reported on a spin-scan tomographical imager. The principle of its operation is shown in Fig. 47 where the imaged scene is rotated over a linear array of parallel elongated detector elements. A unique optical solution, based in part on the construction of a lobster's eye, is proposed for flipping the image. The design of the imager enables measurement of transient processes at speeds above that set by the imager's frame rate.

IR imagers are liable to be blinded by radiation from lasers, explosions, and the sun. One company presented their passive threshold-triggered protection filters, WPF, operating in individual wide spectral bands between the Visible and LWIR. Dual band IR imagers are used for target detection and recognition. The company discussed their choices for protection filters and substrates being optimal for simultaneous operation in MWIR and LWIR bands—see Fig. 48.

The absence of spectral information in a monochrome image obtained with an IR target acquisition system may result in the observer's slow reaction and impaired situational awareness. One company outlined their solution to this critical issue. The company proposed addition of daylight color appearance to the raw monochrome image in order to increase contrast and enable faster and longer range target acquisition. The easy implementation of single band colorization was demonstrated. See example in Fig. 49.

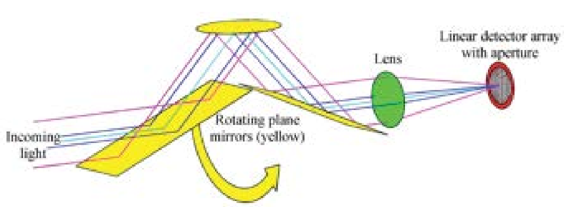

Fig. 47 Spin scan TOSCA imager principle.

Fig. 49 LWIR target image. monochrome above and daylight colorized monochrome below.

Keynote address

.The Keynote address was presented by Dr. Donald Reago, Director of the Night Vision and Electronic Sensors Directorate (NVESD). He reviewed the mission of his organization and key technology thrusts, including:

- Digital low-light sensors
- Micro-displays
- Uncooled technologies
- Digital ROICs
- III-V and II-VI FPA technologies

Efforts also include manufacturing technology programs to move developments into production. Trends in the technology were briefly described.

Paul R. Norton

Bjørn F. Andresen

Gabor F. Fulop

Charles M. Hanson